QUARTERLY JOURNAL OF THE ROYAL METEOROLOGICAL SOCIETY
Q. J. R. Meteorol. Soc. **135**: 1673–1683 (2009)
Published online 1 October 2009 in Wiley InterScience
(www.interscience.wiley.com) DOI: 10.1002/qj.484

RMetS
Royal Meteorological Society

The influence of stratospheric potential vorticity on baroclinic instability

L. A. Smy* and R. K. Scott
University of St Andrews, UK

ABSTRACT: This article examines the dynamical coupling between the stratosphere and troposphere by considering the effect of direct perturbations to stratospheric potential vorticity on the evolution of midlatitude baroclinic instability in a simple extension of an Eady model. A simulation in which stratospheric potential vorticity is exactly zero is used as a control case, and both zonally symmetric and asymmetric perturbations to the stratospheric potential vorticity are then considered, the former representative of a strong polar vortex, the latter representative of the stratospheric state following a major sudden warming. Both types of stratospheric perturbation result in significant changes to the synoptic-scale evolution of surface temperature, as well as to zonally and globally averaged tropospheric quantities. In the case of a zonally symmetric perturbation, the linear growth rate of all unstable modes decreases with increasing perturbation amplitude. Initial growth rates in cases with significant asymmetric perturbations are also weaker than those of the control case, but final eddy kinetic energy values are much larger due to the growth of low zonal wavenumbers triggered by the initial stratospheric perturbation. A comparison of the zonally symmetric and asymmetric perturbations gives some insight into the possible influence of pre- or post-sudden-warming conditions on tropospheric evolution. Copyright © 2009 Royal Meteorological Society

KEY WORDS stratosphere-troposphere dynamical coupling; Eady model; tropospheric evolution

Received 22 December 2008; Revised 7 May 2009; Accepted 3 July 2009

1. Introduction

Observations of correlations between zonally symmetric anomalies of zonal wind and geopotential height in the stratosphere and troposphere (e.g. Kodera *et al.*, 1990; Thompson & Wallace, 1998, 2000; Baldwin & Dunkerton, 1999) have prompted much recent research into the dynamical coupling between these two regions of the atmosphere. These correlations are time-lagged and show tropospheric anomalies that persist on sub-seasonal time-scales, longer than the corresponding stratospheric anomalies. Consequently, it has been suggested that the stratosphere may have a dynamical influence on the tropospheric circulation, even to the extent that medium-range weather forecasts might be improved by improving the representation of the stratosphere in forecast models (Scaife & Knight, 2008).

Dynamical links between the stratosphere and troposphere have been suggested to exist on both sub-seasonal and longer, interannual time-scales. In the latter case, for example, the stratosphere has been shown to influence tropospheric circulation patterns in both comprehensive general circulation models (Hartmann *et al.*, 2000; Shindell *et al.*, 1999, 2001) and simplified primitive equation models (Polvani & Kushner, 2002; Kushner & Polvani, 2004), possibly indicating some sensitivity of the tropospheric circulation to the details of the stratospheric evolution. The stratosphere is now widely believed to play an important role in climate variability (WMO, 2007), although the dynamical processes involved are not well understood.

On shorter time-scales, on the other hand, the strong lag correlations between the strength of the winter stratospheric polar vortex and sea-level pressure distribution (Baldwin & Dunkerton, 1999, 2001; Thompson *et al.*, 2002; Charlton *et al.*, 2003) again point to a dynamical coupling that remains, however, far from well-understood. While descending zonal wind anomalies within the stratosphere can be explained in terms of descending critical layers (Matsuno, 1971), the persistence of tropospheric anomalies on longer time-scales requires the consideration of additional dynamical processes. For example, Song & Robinson (2004) have suggested that stratospheric sudden warming events might couple with the troposphere through an eddy-feedback mechanism. Another recent study by Thompson *et al.* (2006) suggested, on the other hand, that the purely balanced response of the troposphere to changes in stratospheric wave drag and thermal heating may be sufficient to explain longer tropospheric correlation time-scales.

A dynamical link between the stratosphere and troposphere involving the modulation of baroclinic instability by stratospheric zonal wind anomalies has also been considered recently (Wittman *et al.*, 2004, 2007). In simple

*Correspondence to: L. A. Smy, University of St Andrews, UK.
E-mail: lsmy@mcs.st-andrews.ac.uk

baroclinic life-cycle experiments using a general circulation model dynamical core, Wittman *et al.* (2004) found that the strength of the stratospheric zonal winds had an influence on the tropospheric evolution, both in terms of the synoptic-scale development and zonal mean quantities, such as the surface geopotential. Building on this and earlier work by Muller (1991) that examined linear growth rates in a one-dimensional Eady-type model, Wittman *et al.* (2007) further examined the dependence of growth rates on stratospheric shear in a variety of simple and more comprehensive models. In particular, they found that increasing the vertical shear above the tropopause (a representation of a strong stratospheric vortex) increased growth rates across a range of zonal wavenumbers.

In this article, we again investigate the dynamical link between stratospheric anomalies and baroclinic instability, but here restrict attention to anomalies that consist purely of a change to the stratospheric potential vorticity. Our approach is motivated by a recognition of potential vorticity as the principle dynamical quantity governing the slow, balanced motion of the stratosphere. A strong polar vortex is an approximately zonally symmetric distribution of high potential vorticity, while a weak polar vortex may be due either to a distribution of low potential vorticity or, alternatively, to a zonally *asymmetric* distribution of potential vorticity. The latter scenario is the one typically observed during major stratospheric sudden warming events, when strong planetary wave-breaking redistributes the stratospheric potential vorticity, either through a strong displacement of the vortex (in the case of a wave-one warming) or through a vortex split (in the case of a wave-two warming: Charlton & Polvani, 2007). The approach we adopt here allows us to examine in detail how such a redistribution of the stratospheric potential vorticity may affect the tropospheric evolution. Note also that we are interested in resultant changes to the nonlinear tropospheric evolution during the course of a baroclinic life cycle rather than changes to the tropospheric circulation resulting from an instantaneous potential vorticity inversion. The effects of zonal mean perturbations to the stratospheric potential vorticity on the tropospheric circulation as a direct result of potential vorticity inversion were considered by Ambaum & Hoskins (2002) and Black (2002), but not their influence on baroclinic instability.

For simplicity, and to avoid the difficulties involved in balancing an asymmetric potential vorticity distribution, we use a quasi-geostrophic model on an f-plane. The model configuration is described fully in section 2. Baroclinic instability is arranged in the troposphere through an Eady-type distribution of potential temperature at the surface and tropopause. The case in which the stratospheric potential vorticity is exactly zero is treated as a control (discussed in section 3.1). Following this we consider the effect on the instability of zonally symmetric perturbations to the stratospheric potential vorticity (as a representation of a strong vortex, section 3.2) and asymmetric perturbations (as a representation of the vortex following a sudden warming, section 3.3). Finally, we briefly consider the sensitivity of our results to details of the tropospheric mean state (section 3.4).

2. Model description

The numerical model used is the contour-advective semi-Lagrangian (CASL) model developed originally by Dritschel and Ambaum (1997) and extended to cylindrical geometry by Macaskill *et al.* (2003). It solves the quasi-geostrophic equations on an f-plane in a cylindrical domain in uniform rotation about the central axis. One advantage of this model is that it allows easy initialization of both zonal and non-zonal potential vorticity anomalies and a relatively straightforward interpretation of dynamical processes.

In cylindrical coordinates (r, θ, z) the equations take the form

$$\frac{\mathrm{D}q}{\mathrm{D}t} = \frac{\partial q}{\partial t} + \mathbf{u}\cdot\nabla q = 0, \tag{1}$$

$$q = \frac{1}{r}\frac{\partial}{\partial r}\left(r\frac{\partial \psi}{\partial r}\right) + \frac{1}{r^2}\frac{\partial^2 \psi}{\partial \theta^2} + \frac{1}{\rho_0}\frac{\partial}{\partial z}\left(\rho_0 \frac{f_0^2}{N^2}\frac{\partial \psi}{\partial z}\right), \tag{2}$$

$$\mathbf{u} = \left(-\frac{1}{r}\frac{\partial \psi}{\partial \theta}, \frac{\partial \psi}{\partial r}\right), \tag{3}$$

together with an isothermal lower boundary condition $\psi_z = 0$ at $z = 0$. Here q is the (anomalous) quasi-geostrophic potential vorticity, ψ is the geostrophic stream function, and $\mathbf{u} = (u, v)$ is the horizontal geostrophic velocity. The physical parameters are the background density $\rho_0 = \rho_\mathrm{s}\exp(-z/H)$, where H is a vertical scale height and ρ_s is a surface reference density, the 'midlatitude' Coriolis parameter $f_0 = 2\Omega\sin 45^\circ$, where $\Omega = 2\pi$ day^{-1} is the (planetary) rotation rate, and the constant buoyancy frequency N. Numerically, we have chosen $N \approx 0.018$ s^{-1} and $H \approx 8800$ m as being representative of the troposphere, giving a Rossby deformation radius $L_\mathrm{R} = NH/f_0$ of approximately 1525 km.

We use an Eady-type approximation in which the interior tropospheric potential vorticity is uniform and potential vorticity anomalies are concentrated in thin layers near the surface and the tropopause. The standard Eady model has a basic state consisting of a uniform vertical shear $U = \Lambda z$ corresponding to a uniform latitudinal potential temperature gradient $\Theta = -\Lambda y$, together with lower and upper boundary conditions $\psi_z = \theta$ at $z = 0$ and $z = H$. Following Bretherton (1966), this can be recast in terms of the evolution of upper and lower potential vorticity sheets with basic state

$$Q = \Theta\delta(z) - \Theta\delta(z - H), \tag{4}$$

together with isothermal boundary conditions at $z = 0$ and $z = H$. As discussed in Juckes (1994), replacing the upper boundary at $z = H$ with a tropopause separating regions with static stability N_t (tropospheric) and N_s (stratospheric) leads to the same expression but with a

DOI: 10.1002/qj

factor proportional to $(N_t - N_s)/N_t N_s$ multiplying the sheet at $z = H$ (see Equation 3.11 in Juckes, 1994). Since here we are interested in the dynamics of a jet localized in latitude, we generalize the Eady basic state to a non-uniform function of latitude. This motivates the following definition for the total basic state potential vorticity:

$$q = \theta_s(r)\delta(z) - \theta_t(r)\delta(z - H) + q_{strat}, \tag{5}$$

with θ_s and θ_t corresponding to Θ in Equation (4) and where q_{strat} is a basic-state stratospheric potential vorticity, to be specified below.

The initial surface and tropopause potential temperature distributions are specified by a simple latitudinal profile of the form

$$\theta_{s,t}(r) = \Delta\theta_{s,t} \tanh\{(r_j - r)/w\}, \tag{6}$$

of width $2w = L_R$ and centred at $r_j = 4L_R$ (approximately 30° latitude). Analogously to Equation (4), $\Delta\theta_{s,t}$ correspond to the pole–equator potential temperature differences at the surface and tropopause, with $\Delta\theta_s$, $\Delta\theta_t < 0$. The choice $2w = L_R$ is reasonable, being similar to the size of typical eddies developing in a baroclinic flow; the sensitivity of our results to this parameter is described briefly in section 3.4. Choosing values $\Delta\theta_s = -0.2$ and $\Delta\theta_t = -0.6$ gives a basic state comprising a subtropical jet with a maximum $\bar{u}$ of about 35 ms^{-1} and a vertical shear amounting to a difference of about 50 ms^{-1} between the surface and tropopause, as shown in Figure 1(a).

The distribution of potential vorticity in the winter stratosphere is dominated almost entirely by the polar vortex, and may be approximated most simply as a region of high potential vorticity over the Pole and low potential vorticity in midlatitudes. In our model we therefore define q_{strat} by

$$q_{strat}(r, z) = \begin{cases} \Delta Q & \text{if } r < r_v, z \geqslant 1.5H, \\ 0 & \text{otherwise,} \end{cases} \tag{7}$$

where r_v is the vortex radius at a given height and ΔQ is the jump in potential vorticity at the vortex edge. Here the lowermost vortex is situated at a distance of $0.5H$ above the tropopause, as a crude representation of the weaker 'sub-vortex region' and to reduce the direct effect of the stratospheric potential vorticity on the tropospheric winds. It was found that the effect of the polar vortex on the tropospheric evolution is most pronounced when there is no sub-vortex region, and decreases slightly as the region increases in depth. However, the sense of the stratospheric influence is unaffected by the depth of the sub-vortex region, and even the more detailed aspects of the results show very little sensitivity to the depth of the region. Here, we include the sub-vortex region to illustrate that the influence of the polar vortex on the instability is remote, and not due to local interactions in the direct vicinity of the tropopause.

We consider three different forms of r_v to represent typical polar vortex regimes. The simplest form corresponds to a zonally symmetric columnar vortex with $r_v = a$ independent of height. Choosing $a = 2L_R$ gives a polar vortex edge situated near 60° latitude.

The other two forms correspond to a simple horizontal rearrangement of this profile, or deformation of the vortex edge, into a zonally asymmetric state. The first of these takes the form of a simple horizontal displacement of the vortex from over the Pole, similar to a zonal wavenumber-one perturbation. The amplitude of the displacement used for the experiments reported in section 3.3 is such that the vortex is displaced a distance L_R; the dependence of the results on this displacement is also considered. The second asymmetric state is given by a zonal wavenumber-two perturbation of amplitude η to the zonally symmetric state. In polar coordinates, the vortex boundary is displaced from $r_v = a$ (constant) to $r_v = r_v(\theta)$, where

$$r_v(\theta) = \alpha[a + \eta\cos(2\theta)], \tag{8}$$

where the normalization factor $\alpha^2 = a^2/(a^2 + \eta^2/2)$ is included to ensure that the cross-sectional area of the perturbed vortex is the same as that of the zonally symmetric vortex, regardless of η. A disturbance amplitude $\eta = 2$ gives a vortex that is exactly split in a figure-of-eight pattern, while smaller values give a less perturbed vortex. For the results reported in section 3.3 we settled for $\eta = 1$.

The complete tropospheric and stratospheric vorticity distributions are shown in a perspective view in Figure 2. Note that we have added a weak (maximum displacement of $0.1L_D$) zonal wavenumber-six perturbation to the surface and tropopause potential temperature fields to seed the baroclinic instability. This is the fastest-growing mode, and a single-wavenumber perturbation was chosen to allow direct comparison of surface potential temperature fields among different cases during the nonlinear stages of the evolution. The control case, with $q_{strat} = 0$, is shown in Figure 2(a) and the cases with stratospheric perturbation – zonally symmetric, displaced vortex and split vortex – in Figure 2(b)–(d), respectively. The corresponding initial zonal velocity profiles for each case are shown in Figure 1.

The model equations are discretized using 80 layers in the vertical between $z = 0$ and $z = 3H$. This gives a vertical domain extending from the ground to approximately the middle stratosphere. In this problem, the upper stratospheric potential vorticity has practically no impact on details of the tropospheric winds and the evolution of the baroclinic life cycle, so this truncation seems justified. In the horizontal directions, the stream function and velocity fields are calculated on a stretched grid of 128 radial and 264 azimuthal points, although the potential vorticity itself is first interpolated on to a grid four times finer for more accurate inversion. The lateral boundary is located at a distance of $8L_R$ from the Pole and has been verified to have practically no effect on the tropospheric evolution.

Finally, a few words are needed concerning the issue of numerical convergence. In the Eady model, the surface

DOI: 10.1002/qj

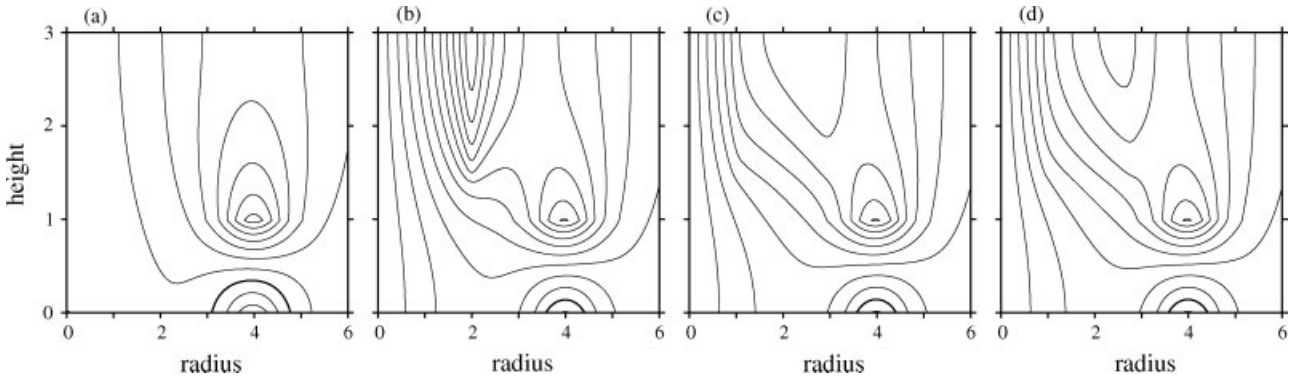

Figure 1. Initial zonal wind profiles of the four main cases: (a) zero stratospheric potential vorticity (the control case), (b) zonally symmetric polar vortex, (c) asymmetric polar vortex (displaced) and (d) asymmetric polar vortex (split). The stratospheric potential vorticity jump in (b)–(d) is $\Delta Q = 0.4f_0$. The contour interval is 5 ms^{-1}. Height is in units of H, radius is in units of L_R.

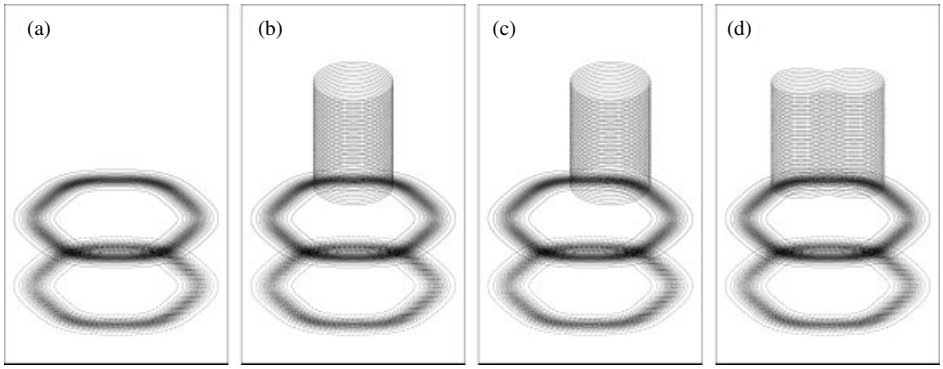

Figure 2. Perspective view of the potential vorticity contours in the four main cases: (a)–(d) as in Figure 1.

and tropopause dynamics exhibit a logarithmic singularity in the tangential velocity field as potential temperature fronts develop (Juckes, 1994). Further, steep potential temperature gradients are a natural feature of the nonlinear evolution during the instability. The logarithmic singularity is here regularized by the fact that the vertical discretization is finite, but increasing the vertical resolution results in increasingly energetic flow at the smallest horizontal scales. It was found by successively doubling both horizontal and vertical resolution together that, although the smallest-scale features of the model continue to exhibit differences at the highest resolution performed, large- and synoptic-scale features are essentially convergent. Further, bulk quantities like the eddy kinetic energy are convergent below the resolution used for the main experiments reported below.

3. Results

3.1. Control

We first briefly describe the control case in which the stratospheric potential vorticity is exactly zero. The initial zonal wind profile for this case is shown in Figure 1(a) and, as described above, comprises a baroclinically unstable subtropical jet with a peak wind speed of approximately 35 ms^{-1} and a vertical shear amounting to a difference of about 50 ms^{-1} between the surface and tropopause.

The growth of the instability is such that significant nonlinearity develops by around days 6–8 of the evolution, with eddy kinetic energy peaking near day 10 and then decreasing again in a decay stage, the classic baroclinic life-cycle paradigm. The synoptic surface potential temperature distribution for the control case at days 10, 12 and 14 of the life-cycle evolution is shown in Figure 3(a)–(c). Significant nonlinearity has developed by day 10 with the usual wave-breaking, irreversible mixing of potential vorticity and intensification of potential temperature gradients. Because of the simplicity of our model, only a very qualitative comparison of this evolution with that observed in more sophisticated models is possible. However, the evolution can be regarded as broadly similar to the LC1 life cycle of Thorncroft *et al.* (1993) with predominantly anticyclonic equatorward wave-breaking during the saturation phase. Examination of the zonal mean zonal velocity and wave fluxes (not shown) indicates a transfer of energy into a deeper barotropic jet and an upward wave flux from the surface to the tropopause.

3.2. Zonally symmetric perturbation

To examine the effect of stratospheric potential vorticity on the tropospheric evolution, we next consider cases with non-zero q_{strat}. We first consider the case of a zonally symmetric perturbation to the stratospheric potential vorticity. More realistic perturbations will follow in

DOI: 10.1002/qj

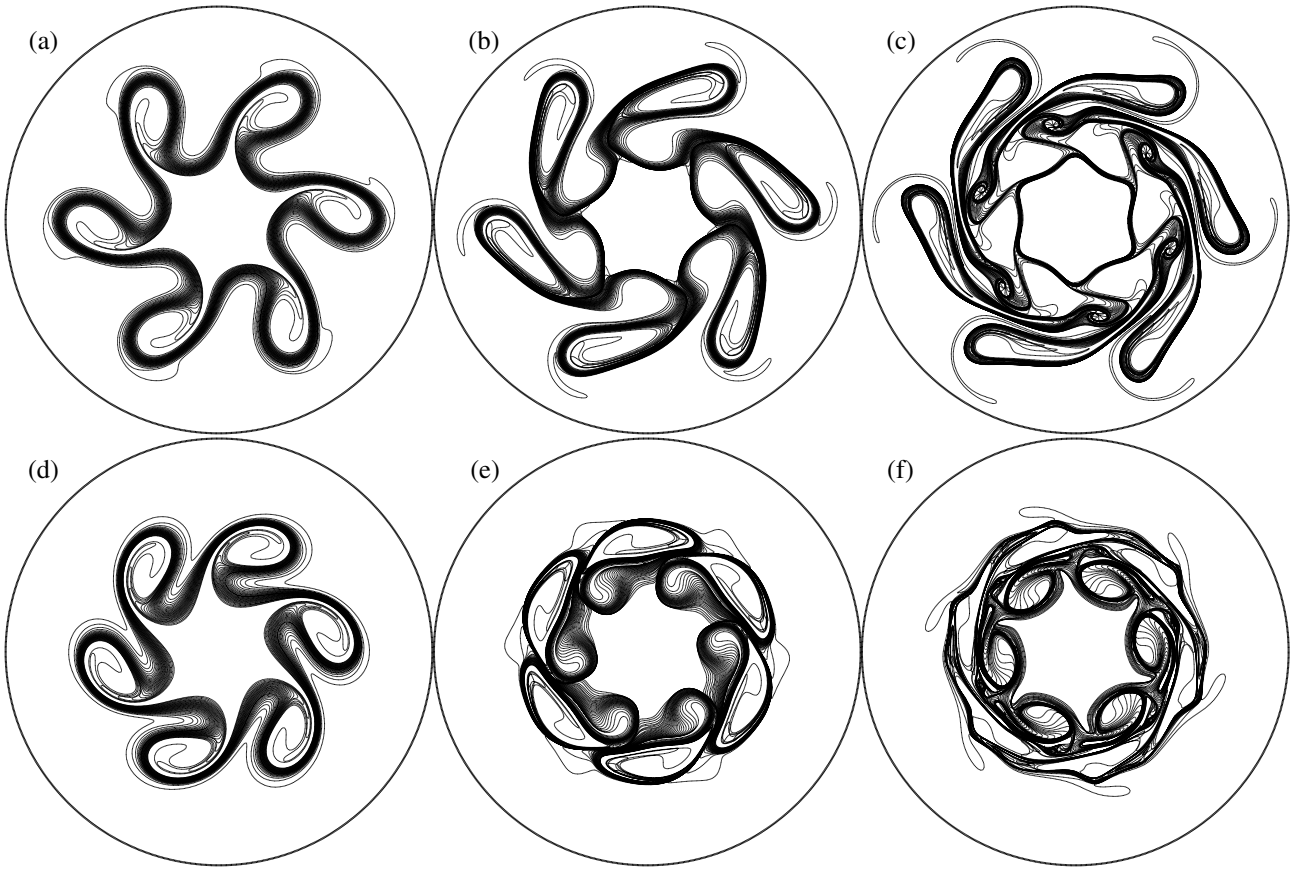

Figure 3. Surface potential temperature at days 10, 12 and 14: (a)–(c) the control case $\Delta Q = 0$, and (d)–(f) with a zonally symmetric stratospheric anomaly of $\Delta Q = 0.4 f_0$.

section 3.3, but we note for now that a zonally symmetric perturbation can be regarded as a crude representation of a strong polar vortex, and can therefore be contrasted with the control case discussed above (which can be regarded as an extreme example of a weak vortex). Our comparison here is similar to the situation considered by Wittman *et al.* (2004), who restricted attention to purely zonally symmetric initial conditions, with or without a stratospheric polar vortex.

The zonally symmetric perturbation to the stratospheric potential vorticity is defined by Equation (7) with $r_v = a = 2L_R$. Here we focus on the case $\Delta Q = 0.4 f_0$, which gives rise to a relatively strong polar vortex (in terms of $\bar{u}$ near the vortex edge), but the intermediate case of $\Delta Q = 0.2 f_0$ is also discussed briefly. As can be seen in Figure 1, the addition of the polar vortex in the stratosphere has a direct effect on the initial-state tropospheric zonal wind due to potential vorticity inversion. Note, however, that although the tropospheric jet has increased to a maximum of 45 ms^{-1} (compared with 35 ms^{-1} in the control), the vertical shear between the surface and tropopause is largely unchanged. In contrast, the addition of the polar vortex results in a more significant change to the horizontal shear throughout the troposphere, which has a subsequent effect on the tropospheric evolution.

Figure 3(d)–(f) shows the synoptic surface potential temperature evolution for the zonally symmetric perturbation with $\Delta Q = 0.4 f_0$ at days 10, 12 and 14. Again, the baroclinic instability results in wave-breaking and irreversible mixing across the jet. However, in the perturbed case increased horizontal shear throughout the troposphere results in an eddy growth that is now more confined in latitude than before. This interpretation is consistent with the results of Thorncroft *et al.* (1993), where the addition of barotropic shear to the initial mean zonal flow of an LC1 life cycle resulted in significantly different nonlinear dynamics (the LC2 life cycle). While interpretation of the evolution shown in Figure 3 in terms of LC1 and LC2 life cycles is difficult, owing to the simplicity of our model, there are nevertheless clear differences between the two cases. For example, both the strong equatorward wave-breaking of the control case and the weaker, poleward wave-breaking are attenuated in the case with $\Delta Q = 0.4 f_0$. At later times, days 12–14, the poleward breaking in the control case results in strong transport of low-latitude air into high latitudes, which is much weaker in the perturbation case.

To quantify the change in eddy growth with changes to the stratospheric potential vorticity, we show in Figure 4 the eddy kinetic energy as a function of time for the case of exactly zero stratospheric potential vorticity (the control, for which $\Delta Q = 0$) and two cases with increasing strength of stratospheric potential vorticity anomalies, $\Delta Q = 0.2 f_0$ and $\Delta Q = 0.4 f_0$. At early times there is a decrease in the growth rate of eddy kinetic energy with increasing ΔQ, and, consequently, a reduction in

DOI: 10.1002/qj

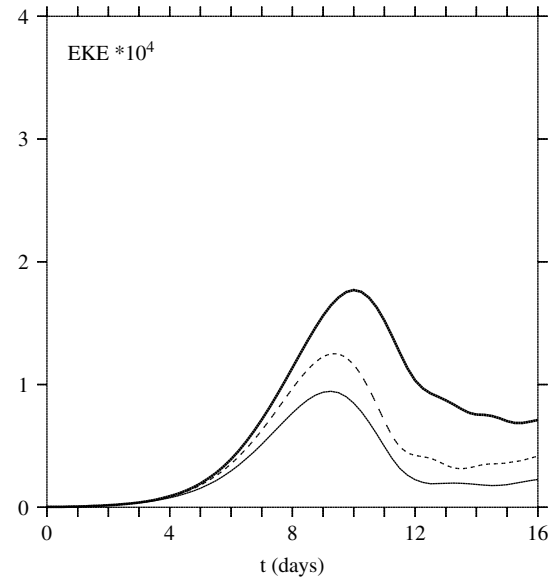

Figure 4. Eddy kinetic energy as a function of time for the cases with a zonally symmetric polar vortex with $\Delta Q = 0$ (bold solid line), $\Delta Q = 0.2 f_0$ (dashed line) and $\Delta Q = 0.4 f_0$ (thin solid line).

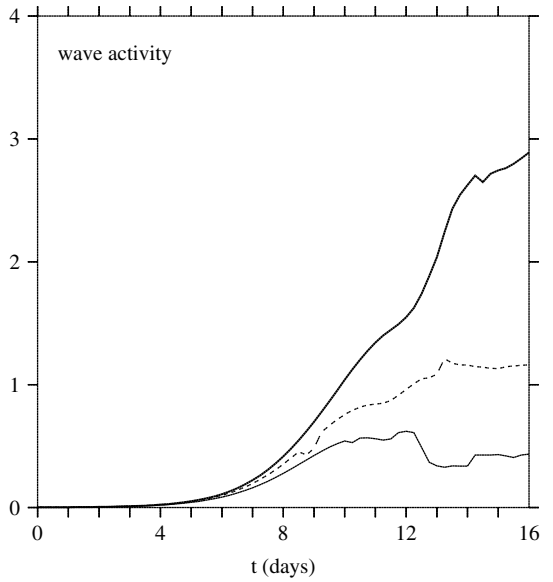

Figure 5. Combined surface and tropopause wave activity as a function of time for the cases $\Delta Q = 0$ (bold solid line), $\Delta Q = 0.2 f_0$ (dashed line) and $\Delta Q = 0.4 f_0$ (thin solid line). Values have been normalized by the initial angular impulse of the case $\Delta Q = 0$.

the maximum value obtained around day 10. At first sight, this dependence might appear contrary to the results of Wittman *et al.* (2007), who found using a primitive equation model that the growth rate of eddy kinetic energy increased monotonically (at wavenumbers less than 7) with increasing vertical shear in the stratosphere, their proxy for the polar vortex. In fact, the two sets of results appear to be consistent when we take into account the details of the changes to the initial shear caused by the stratospheric perturbations in each case. In Wittman *et al.*, the addition of vertical shear in the stratosphere appears to enhance the eddy growth rate in a similar way as increasing the vertical shear in the troposphere in the traditional Eady model. In our model, on the other hand, the addition of the stratospheric potential vorticity anomaly has practically no effect on the vertical shear in the troposphere or anywhere near the subtropical jet (Figure 1(a) and (b)). As discussed above, however, it does increase the horizontal shear throughout the troposphere, with a resultant change in the character of the life cycle, consistent with Thorncroft *et al.* (1993). Of course, other differences between the two modelling frameworks (e.g. cylindrical versus spherical geometry, quasi-geostrophic versus primitive equations, latitudinal offset between the polar vortex and the subtropical jet) may also alter details of the evolution. However, the dependence of the growth rates on the tropospheric shear would appear to be consistent.

Another useful measure of eddy growth, particularly suited to the contour representation used here, is the wave activity A, defined as

$$A(z,t) = \frac{1}{4}\rho_0(z) \sum_k q_k \oint_{\Gamma_k(z)} \left(r^2 - r_e^2\right)^2 \, \mathrm{d}\theta, \qquad (9)$$

where the sum is over all contours Γ_k in a given vertical level, where r_e is the radius of the undisturbed circular contour enclosing the same area as Γ_k and q_k is the vorticity jump on the kth contour. This is a nonlinear pseudo-momentum-based wave activity, second-order in disturbance amplitude, satisfying an exact conservation relation (see Dritschel, 1988 and Dritschel & Saravanan, 1994 for more details). The evolution of total wave activity contained in the surface and tropopause potential temperature fields is shown in Figure 5 for the three cases $\Delta Q = 0,\ 0.2 f_0,\ 0.4 f_0$. Like the eddy kinetic energy, the wave activity increases due to the instability, and again with weaker growth at higher values of ΔQ. At late times the difference between the cases is even more marked, with continued increase in the wave activity in the case $\Delta Q = 0$ but not in the other cases. We note incidentally that these differences in the tropospheric wave activity are entirely due to the evolution of the basic instability: the amount of wave activity 'leaking' from the troposphere into the polar vortex is negligible, with values of the stratospheric wave activity remaining around five orders of magnitude less than tropospheric values throughout the evolution.

As in Wittman *et al.* (2004), it is also possible to consider the surface geopotential height difference as a crude measure of the extent to which the instability projects on to the Arctic Oscillation. Figure 6 shows the difference between the surface geopotential height anomaly at day 12 and day 0. The magnitude of the dipole structure resulting from the instability becomes weaker for larger values of ΔQ, consistent with the reduction of eddy growth rates discussed above. Again the difference in dependence on ΔQ from that found in Wittman *et al.* (2004) can be understood in terms of changes to the tropospheric shear induced by the stratospheric perturbation.

DOI: 10.1002/qj

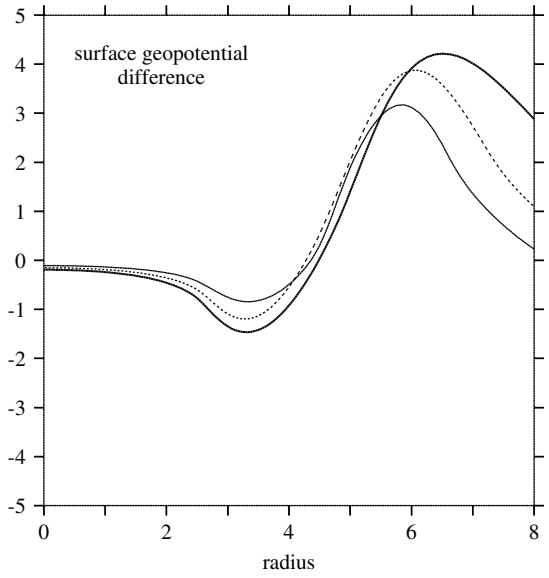

Figure 6. Difference between the surface geopotential at day 12 and day 0 for the cases $\Delta Q = 0$ (bold solid line), $\Delta Q = 0.2 f_0$ (dashed line) and $\Delta Q = 0.4 f_0$ (thin solid line).

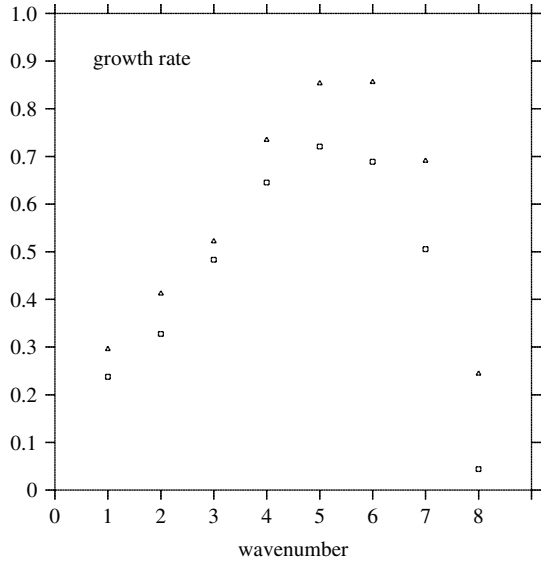

Figure 7. The linear growth rate of eddy kinetic energy with different initial wavenumber perturbations in the troposphere: triangles correspond to the control case, $\Delta Q = 0$, and squares correspond to a zonally symmetric stratospheric polar vortex with $\Delta Q = 0.4 f_0$.

Finally, we examine the effect of the stratospheric perturbation on the growth rate of other wavenumber disturbances to the surface and tropopause basic state. Here we consider the difference between the two cases $\Delta Q = 0$ and $\Delta Q = 0.4 f_0$ and calculate the linear growth rates of different wavenumbers by integrating the model at early times only. One reason for doing so is to verify that the addition of a polar vortex indeed reduces the growth rate at all wavenumbers rather than simply shifting the wavenumber of the fastest-growing mode. As seen in Figure 7, this is indeed the case, with a modest reduction in growth rate across all wavenumbers.

3.3. Asymmetric perturbations

We now consider the effect of asymmetric perturbations to the stratospheric potential vorticity on the tropospheric evolution. Again, these perturbations are representative of the shape of the polar vortex following a stratospheric sudden warming. Here, we focus on the displaced vortex case (a wave-one warming) but note that very similar results were also obtained in the case of a split vortex.

As before, the stratospheric perturbation has an instantaneous effect through potential vorticity inversion on the tropospheric basic state, as shown in Figure 1(c) and (d) for the displaced and split-vortex cases with $\Delta Q = 0.4 f_0$. However, in comparison with Figure 1(b), we see that the biggest differences in the winds between the symmetric and asymmetric vortex cases are in the stratosphere: because the asymmetric perturbation results in a latitudinally distributed zonal mean stratospheric potential vorticity, the stratospheric jet is also broader and weaker than in the case with a zonally symmetric vortex. In the troposphere, on the other hand, the winds are very similar in all cases (symmetric, displaced vortex and split vortex), in almost all respects, including the maximum of the subtropical jet and the vertical and horizontal shear. Thus the *instantaneous* effect of a rearrangement of the stratospheric potential vorticity on the tropospheric zonal flow is very small.

Figure 8 shows the synoptic surface potential temperature evolution at days 10, 12 and 14 for the case $\Delta Q = 0.4 f_0$ and a vortex displacement of distance L_R. What is immediately apparent is the strong departure from six-fold symmetry, which results from the interaction of the fastest-growing wave-six mode in the troposphere with the growth of wave one initiated by the displaced polar vortex. Although the growth rate of wave one is much smaller than that of wave six (Figure 7), the wave-one perturbation induced by the displaced polar vortex is larger than the initial wave-six tropospheric perturbation, with the result that significant growth of wave one occurs. This growth is naturally smaller for smaller initial displacements of the polar vortex; however, it was found that even relatively small displacements (down to a distance of $0.2 L_R$) were sufficient to cause significant development of a tropospheric wave one by day 16 (with gradually later development at smaller displacement values). Thus a simple displacement of the polar vortex may have a significant effect on the tropospheric evolution.

The growth of eddy kinetic energy for the control case ($\Delta Q = 0$) and the two cases $\Delta Q = 0.2 f_0$ and $\Delta Q = 0.4 f_0$ (with a vortex displacement of L_R) is shown in Figure 9. The contribution of the initial stratospheric polar vortex displacement is evident in the eddy kinetic energy at $t = 0$. Despite these larger initial values, however, growth rates during the development of the instability are smaller at larger values of ΔQ, similar to the case of a zonally symmetric stratospheric perturbation. Essentially, the eddy growth at early times is again dominated by the fastest-growing mode, despite the presence of the large wave-one perturbation. This behaviour changes dramatically at later times, however, when the growth

DOI: 10.1002/qj

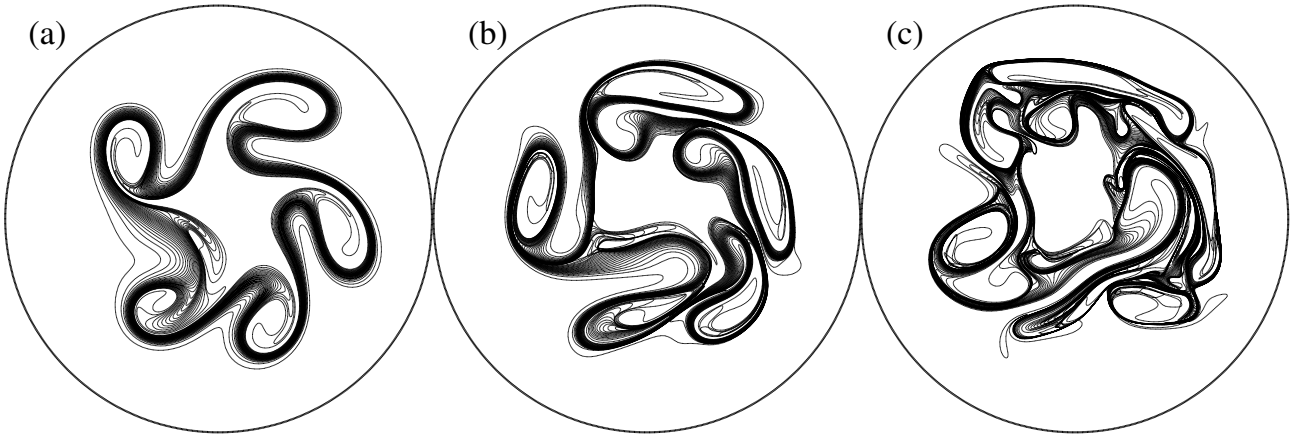

Figure 8. Surface potential temperature at days 10, 12 and 14 for the case of a displaced polar vortex (centred at $r = L_R$) with $\Delta Q = 0.4 f_0$.

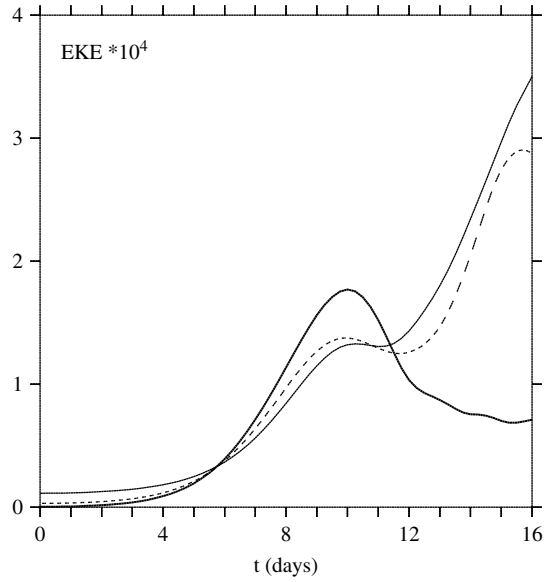

Figure 9. Eddy kinetic energy as a function of time for a displaced polar vortex (centred at $r = L_R$) with $\Delta Q = 0$ (bold solid line, same as the control case), $\Delta Q = 0.2 f_0$ (dashed line) and $\Delta Q = 0.4 f_0$ (thin solid line).

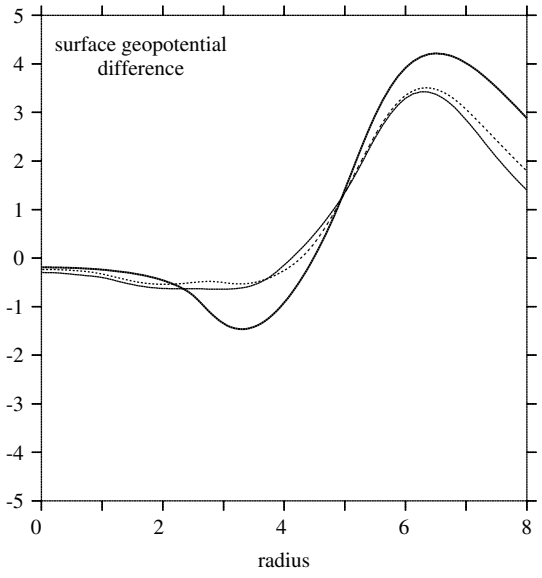

Figure 10. Difference between the surface geopotential height at day 12 and day 0 for the displaced polar vortex (centred at $r = L_R$) with $\Delta Q = 0$ (bold solid line), $\Delta Q = 0.2 f_0$ (dashed line) and $\Delta Q = 0.4 f_0$ (thin solid line).

of the wave-one perturbation eventually overtakes that of the wave-six one: whereas saturation of wave six occurs around day 10, saturation of wave one does not occur until around day 16 or later, at significantly higher values of eddy kinetic energy. The evolution for the case of the split vortex (not shown) is qualitatively very similar to that of the displaced vortex, with large eddy growth due to the development of wave two dominating at late times. Eddy kinetic energy plots for this case are similar to those shown in Figure 9, while the surface potential temperature fields show the late time development of wave four due to the interaction of the wave-six and wave-two initial perturbations.

Instead of comparing the tropospheric evolution at different ΔQ, it is perhaps more instructive to consider the differences between the zonally symmetric and displaced polar vortex cases, both with $\Delta Q = 0.4 f_0$, the potential vorticity in the displaced vortex case being simply a redistribution of that in the symmetric case. The surface potential temperature fields (compare Figure 3(d)–(f) and Figure 8) are significantly different between the two cases already at day 10, but still more so at late times, when much more vigorous mixing is found across a wider latitudinal region in the displaced vortex case. Similarly, the eddy kinetic energy shows significant differences at late times (compare the thin solid lines in Figures 4 and 9), although growth rates at early times are similar.

The more vigorous mixing across latitude has an influence on the zonal mean surface geopotential height anomalies considered above. Figure 10 again shows the difference between the surface geopotential height anomaly at day 12 and day 0, for $\Delta Q = 0$, $0.2 f_0$, $0.4 f_0$ but for the displaced vortex cases. As in the case of the zonally symmetric vortex, large ΔQ again results in a less pronounced dipolar structure in midlatitudes. Comparing the thin solid line in this figure with that in Figure 6 indicates that the redistribution of potential vorticity in the stratosphere has also had an effect on

DOI: 10.1002/qj

the resulting surface geopotential height following the baroclinic development.

Finally, it is again useful to consider the evolution of wave activity in these cases. At $t = 0$, the stratospheric wave activity (not shown) due to the displaced vortex is around four times that due to the initial tropospheric wave-six perturbation. This stratospheric wave activity decreases until around day 8 due to downward wave propagation (Scott & Dritschel, 2005) and is the source for the subsequent growth of wave one in the troposphere. However, the initial stratospheric wave activity is much smaller than the subsequent difference in the tropospheric wave activity between the zonally symmetric and displaced vortex cases, which can only be accounted for by the unstable growth of wave one, and not by simple downward propagation of waves from the stratosphere. Final (day 16) values of stratospheric wave activity are around four times larger than initial ones, indicating that some of the wave-one development in the troposphere is subsequently able to propagate upwards on the polar vortex edge (in contrast to wave six, which, as discussed above, is trapped in the troposphere).

3.4. Influence of the basic state

To verify that the above results are not sensitive to details of the tropospheric initial conditions, we have performed a number of variations with different values for the surface and tropopause $\Delta\theta$ and different forms of the latitudinal profiles, as well as different relative positions of the polar vortex and subtropical jet. In all cases the results are broadly similar to those reported above, with increasing stratospheric potential vorticity perturbation resulting in weaker eddy growth in the troposphere, related to changes in horizontal shear. In this section we briefly describe a few a these variations.

In one variation we consider a surface potential temperature distribution that has a broader latitudinal structure, with $2w = 4L_R$ for the surface distribution (and $2w = L_R$ at the tropopause as before). This gives a slightly more realistic zonal wind profile, as shown in Figure 12(a) and (b) for the cases of no polar vortex and a zonally symmetric polar vortex with $\Delta Q = 0.4 f_0$. The zonal winds are now increasing monotonically at all heights between the pole and the jet latitude, and decreasing equatorward of the jet, and, in particular, there is now a surface shear that is cyclonic poleward of the jet latitude, closer to the observed zonal wind profile (compare this with Figure 1(a), where the shear just poleward of the jet location is anticyclonic). This could be important, for instance in determining the direction of synoptic wave-breaking during the evolution of the life cycle, where, for example, the poleward wave-breaking in Figure 3 appears initially anticyclonic. We emphasize, however, that here we are less interested in the details of the synoptic development than on the influence of the polar vortex on the overall growth rate of the instability.

Figure 11 shows the surface potential vorticity at day 14 for three cases: (a) with $\Delta Q = 0$, similar to the control case discussed above; (b) with $\Delta Q = 0.4 f_0$ and a zonally symmetric vortex; (c) with $\Delta Q = 0.4 f_0$ and a vortex that has been displaced horizontally by a distance L_R. The corresponding figures from the previous cases are the right-hand panels in Figures 3 and 8. The increase in cyclonic meridional shear poleward of the jet has resulted in slower growth of the instability across all cases, although the poleward breaking remains initially anticyclonic. However, and more importantly, the difference between cases remains much the same as before. In terms of both eddy kinetic energy and wave activity (not shown), the largest growth is again for the case $\Delta Q = 0$, while in the cases with $\Delta Q = 0.4 f_0$ the case of the displaced vortex again exhibits larger eddy growth at late times than the case of the zonally symmetric vortex.

In a second variation we considered the effect of simply adding a r-dependent barotropic shear to the initial state, similar to the LC2 life cycle case considered in Thorncroft *et al.* (1993). The resulting initial zonal wind profiles are broadly similar to those shown in Figure 12, as is the subsequent evolution (not shown). In particular, we again found a robust decrease in the growth rate of the instability when the polar vortex was added, and a late time increase in eddy kinetic energy in the displaced vortex case due to the growth of low wavenumbers.

Finally, we considered a basic state characterized by two surface temperature fronts located poleward and equatorward of jet latitude. Such a distribution arises naturally as a result of eddy mixing of surface temperature due to baroclinic waves, and can be considered to represent the statistically stationary state of the atmosphere. This state would also be obtained by zonally averaging the final temperature distributions in the above calculations. For completeness, therefore, we repeated the main series of experiments using this tropospheric basic state, although it could be argued that such a state is not the most appropriate choice of initial conditions in the life-cycle approach. In fact, we found that the details of this surface-temperature basic state made very little difference to the influence of the polar vortex on the instability, with an increase in polar vortex strength again resulting in a decrease in growth rate. Overall, it appears therefore that the influence of the polar vortex on the evolution is insensitive to details of the initial basic state, at least within the limitations of our restricted model.

4. Discussion

To summarize our results, changes to the stratospheric potential vorticity have a significant impact on the development of baroclinic instability in an Eady-like model. The dependence is such that increasing the strength of the polar vortex tends to decrease the eddy growth in the troposphere. This is found not just in the zonally symmetric cases, comparing zonally symmetric stratospheric perturbations of different potential vorticity magnitudes, but also in cases of zonally asymmetric disturbances to a

DOI: 10.1002/qj

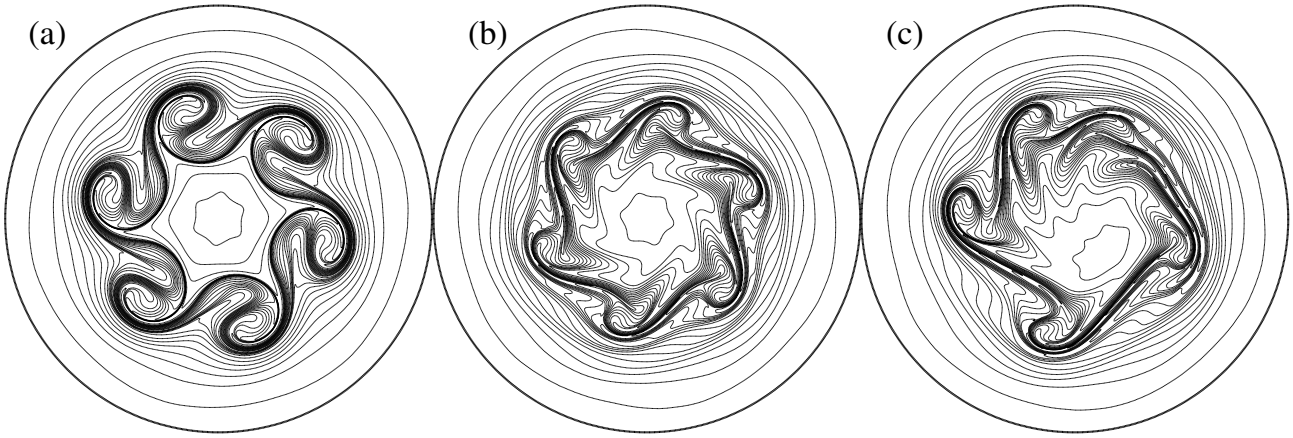

Figure 11. Surface potential temperature at day 14 for the case with broad surface-temperature initial condition: (a) $\Delta Q = 0$ (the control); (b) a zonally symmetric vortex with $\Delta Q = 0.4f_0$; (c) a displaced polar vortex (centred at $r = L_R$) with $\Delta Q = 0.4f_0$.

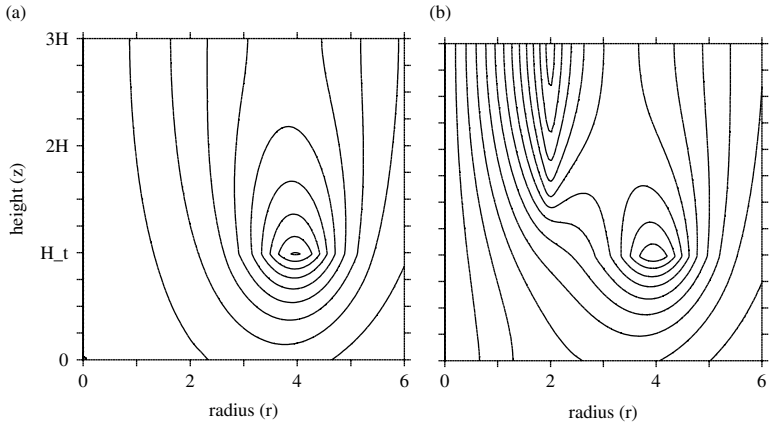

Figure 12. Initial zonal wind profiles for the case with broad surface-temperature initial condition: (a) $\Delta Q = 0$ (the control); (b) a zonally symmetric vortex with $\Delta Q = 0.4f_0$. The contour interval is 5 ms^{-1}.

polar vortex of given potential vorticity. The latter scenario extends previous work that considered only zonally symmetric stratospheric perturbations. In particular, we found that there is a large difference in the tropospheric evolution between cases representing a strong vortex and cases representing the vortex following either a wave-one or wave-two sudden warming. Differences in the tropospheric evolution include the growth of eddy kinetic energy and wave activity, as well as synoptic-scale details of the wave-breaking and the latitudinal extent of mixing within the troposphere.

Our study differs fundamentally in philosophy from the related work of Wittman *et al.* (2004, 2007), in which perturbations were made to the stratospheric zonal winds. It is of course true that by perturbing the stratospheric potential vorticity, as is done here, one is also perturbing the tropospheric zonal flow. However, because of the fundamental nature of the potential vorticity (Hoskins *et al.*, 1985) it is perhaps justified to consider such stratospheric potential vorticity perturbations as dynamical perturbations to the stratosphere only. In our case, these perturbations have been carefully isolated from the troposphere by including a 'sub-vortex' region between the troposphere and lowermost polar vortex, in which the potential vorticity is unperturbed. Moreover, actual differences in the initial tropospheric zonal winds between zonally symmetric and asymmetric perturbation cases are very slight (compare Figure 1(b)–(d)). Finally, this kind of perturbation is arguably closer to the situation resulting from a stratospheric sudden warming. One of the important results of the present article is that the potential vorticity perturbations made here result in significantly larger differences to the tropospheric evolution than obtained by perturbations to the stratospheric winds alone.

One significant difference between our results and those of Wittman *et al.*, is the sense in which a stratospheric perturbation affects the growth of the instability. Wittman *et al.*, found an increase in eddy growth rates with increasing stratospheric shear, whereas we find a decrease in growth rates with increasing stratospheric potential vorticity. The results are not inconsistent when full account is taken of changes to the tropospheric shear resulting from the stratospheric potential vorticity perturbation in our case, which tends to leave the vertical shear unchanged but increases the horizontal shear. The decrease in growth rates we observed may therefore be attributed to a change in the nature of the baroclinic development similar to that found by Thorncroft *et al.* (1993).

DOI: 10.1002/qj

One conclusion that may be drawn from both Wittman *et al.*, and the present work is that the tropospheric evolution depends rather sensitively on the stratospheric state through details of the shear in the troposphere and near the subtropical jet.

Acknowledgements

The authors wish to thank Andrew Charlton, David Dritschel, and Lorenzo Polvani for useful comments and discussions during the preparation of this manuscript. Financial support was provided through an EPSRC CASE studentship with the UK Meteorological Office.

References

Ambaum MHP, Hoskins BJ. 2002. The NAO troposphere–stratosphere connection. *J. Climate* **15**: 1969–1978.

Baldwin MP, Dunkerton TJ. 1999. Propagation of the Arctic oscillation from the stratosphere to the troposphere. *J. Geophys. Res.* **104**: 30 937–30 946.

Baldwin MP, Dunkerton TJ. 2001. Stratospheric harbingers of anomalous weather regimes. *Science* **294**: 581–584.

Black RX. 2002. Stratospheric forcing of surface climate in the Arctic oscillation. *J. Climate* **15**: 268–277.

Bretherton FP. 1966. Critical layer instability in baroclinic flows. *Q. J. R. Meteorol. Soc.* **92**: 325–334.

Charlton AJ, Polvani LM. 2007. A new look at stratospheric sudden warmings. Part I. Climatology and modeling benchmarks. *J. Climate* **20**: 449–469.

Charlton AJ, O'Neill A, Stephenson DB, Lahoz WA, Baldwin MP. 2003. Can knowledge of the state of the stratosphere be used to improve statistical forecasts of the troposphere? *Q. J. R. Meteorol. Soc.* **129**: 3205–3224.

Dritschel DG. 1988. Contour surgery: A topological reconnection scheme for extended integrations using contour dynamics. *J. Comp. Phys.* **77**: 240–266.

Dritschel DG, Ambaum MHP. 1997. A contour-advective semi-Lagrangian numerical algorithm for simulating fine-scale conservative dynamical fields. *Q. J. R. Meteorol. Soc.* **123**: 1097–1130.

Dritschel DG, Saravanan R. 1994. Three-dimensional quasi-geostrophic contour dynamics, with an application to stratospheric vortex dynamics. *Q. J. R. Meteorol. Soc.* **120**: 1267–1297.

Hartmann DL, Wallace JM, Limpasuvan V, Thompson DWJ, Holton JR. 2000. Can ozone depletion and global warming interact to produce rapid climate change? *Proc. Nat. Acad. Sci. (Wash. DC)* **97**: 1412–1417.

Hoskins BJ, McIntyre ME, Robertson AW. 1985. On the use and significance of isentropic potential vorticity maps. *Q. J. R. Meteorol. Soc.* **111**: 877–946.

Juckes MN. 1994. Quasigeostrophic dynamics of the tropopause. *J. Atmos. Sci.* **51**: 2756–2768.

Kodera K, Yamazaki K, Chiba M, Shibata K. 1990. Downward propagation of upper stratospheric mean zonal wind perturbation to the troposphere. *Geophys. Res. Lett.* **17**: 1263–1266.

Kushner PJ, Polvani LM. 2004. Stratosphere–troposphere coupling in a relatively simple AGCM: The role of eddies. *J. Climate* **17**: 629–639.

Macaskill C, Padden WEP, Dritschel DG. 2003. The CASL algorithm for quasi-geostrophic flow in a cylinder. *J. Comp. Phys.* **188**: 232–251.

Matsuno T. 1971. A dynamical model of the stratospheric sudden warming. *J. Atmos. Sci.* **28**: 1479–1494.

Muller JC. 1991. Baroclinic instability in a two-layer, vertically semi-infinite domain. *Tellus A* **43**: 275–284.

Polvani LM, Kushner PJ. 2002. Tropospheric response to stratospheric perturbations in a relatively simple general circulation model. *Geophys. Res. Lett.* **29**: 1114. DOI: 10.1029/2001GLO14284

Scaife AA, Knight JR. 2008. Ensemble simulations of the cold European winter of 2005–2006. *Q. J. R. Meteorol. Soc.* **134**: 1647–1659.

Scott RK, Dritschel DG. 2005. Downward wave propagation on the polar vortex. *J. Atmos. Sci.* **62**: 3382–3395.

Shindell DT, Rind D, Balachandran N, Lean J, Lonergan P. 1999. Solar cycle variability, ozone, and climate. *Science* **284**: 305–308.

Shindell DT, Schmidt GA, Mann ME, Rind D, Waple A. 2001. Solar forcing of regional climate change during the Maunder minimum. *Science* **294**: 2149–2152.

Song Y, Robinson WA. 2004. Dynamical mechanisms for stratospheric influences on the troposphere. *J. Atmos. Sci.* **61**: 1711–1725.

Thompson DWJ, Wallace JM. 1998. The Arctic oscillation signature in the wintertime geopotential height and temperature fields. *Geophys. Res. Lett.* **25**: 1297–1300.

Thompson DWJ, Wallace JM. 2000. Annular modes in the extratropical circulation. Part 1: Month-to-month variability. *J. Climate* **13**: 1000–1016.

Thompson DWJ, Baldwin MP, Wallace JM. 2002. Stratospheric connection to northern hemisphere wintertime weather: Implications for prediction. *J. Climate* **15**: 1421–1428.

Thompson DWJ, Furtado JC, Shepherd TG. 2006. On the tropospheric response to anomalous stratospheric wave drag and radiative heating. *J. Atmos. Sci.* **63**: 2616–2629.

Thorncroft CD, Hoskins BJ, McIntyre ME. 1993. Two paradigms of baroclinic-wave life-cycle behaviour. *Q. J. R. Meteorol. Soc.* **119**: 17–55.

Wittman MAH, Polvani LM, Scott RK, Charlton AJ. 2004. Stratospheric influence on baroclinic lifecycles and its connection to the Arctic oscillation. *Geophys. Res. Lett.* **31**: L16113.

Wittman MAH, Charlton AJ, Polvani LM. 2007. The effect of lower stratospheric shear on baroclinic instability. *J. Atmos. Sci.* **64**: 479–496.

WMO. 2007. *'Scientific assessment of ozone depletion: 2006'*, WMO Global Ozone Research and Monitoring Project Report No. 50. World Meteorol. Org.: Geneva.